Analysis of a Chirp-Based Waveform for Joint Communications and Radar Sensing (JC&S) using Non-Linear Components

Andre N. Barreto, Thuy M. Pham, Sandra George, Padmanava Sen and Gerhard Fettweis

Barkhausen Institut, Dresden, Germany
Email: {andre.nollbarreto, minhthuy.pham, sandra.george, padmanava.sen, gerhard.fettweis}@barkhauseninstitut.org

***Abstract*—Joint communications and radar sensing (JC&S) is expected to be one of the key features in beyond 5G (B5G) networks, allowing the provision of radar as a service (RaaS). In this paper, we are interested in a chirp-based waveform that can be effectively employed for both communication and radar applications. More specifically, we investigate the performance of such a waveform in the presence of realistic non-linear power amplifiers (PA) and low-noise amplifiers (LNA), operating at mmWave frequencies.**

I. Introduction

Sensing is widely seen as one of the key technologies in the sixth generation (6G) of wireless communication systems [1], allowing a plethora of new services and applications. It is envisaged that radar sensing, in particular, will be integrated with the communications network [2], such that it can be offered as an additional service upon demand, in what we call Radar as a Service (RaaS).

Currently, radar and wireless communication systems are designed and deployed separately, using different hardware and waveforms, and distinct parts of the spectrum. Consumer radar applications, especially for the automotive industry, currently operate mostly in the 24 GHz and in the 76-81 GHz bands, with the former being discontinued soon [3]. Anyway, there will still be 5 GHz of spectrum being used for automotive and consumer-market radar, not to mention the spectral allocation for aeronautical, meteorological and military radar. This is nearly twice as much as the whole 5G spectrum currently available, including the frequencies above 6 GHz. Radar services are already extensively used in vehicles, and their usage is likely to increase with new autonomous vehicles, but this usage is currently limited to highways and streets. Other usages of radar can be envisaged, like gesture recognition [4], but in most places, like homes, offices and parks, this sizeable portion of the spectrum remains largely unexploited.

There have been some attempts in the literature to allow the coexistence of both systems [5] in the same spectrum band using cognitive-radio techniques. This approach can be effective when we have an incumbent primary service at fixed locations, but it is unlikely to make full usage of the available spectral resources in a more dynamic scenario. Also, in this approach, radar and communications are still considered as separate systems, using different waveforms and equipment.

However, it is common knowledge that both applications rely on the same physical phenomenon, i.e., the propagation of electromagnetic waves, and, therefore, both radar sensing and wireless communications could be co-designed, such that they can share the same waveform, spectrum and hardware.

This latter approach allows a flexible allocation of resources, depending on the temporal and spatial needs of each service, which results in a more efficient usage of the available spectrum. For instance, in a busy street crossing, most of the resources can be allocated to radar, whereas at home the spectrum can be fully allocated for communications, to allow communications at very high data rates. The service demands may also dynamically vary over time. For example, a radar application may consist of several distributed radars in different vehicles and in the infrastructure, which communicate with each other through an in-band broadband communications link, for interference coordination and/or sensor fusion.

One of the research challenges towards this vision is how to design a physical layer (PHY) that is flexible, but still efficient for both radar and communications. Orthogonal frequency-division multiplexing (OFDM) has been proposed as a possible waveform [6], but its implementation can be rather complex for the large bandwidths under consideration, and would also require full duplexing terminals for monostatic radars.

In fact, a chirp-based waveform can be effectively used to achieve both functionalities. Chirps are extensively used in radar systems, because of their good ambiguity properties, but mostly because of the possibility of a less-complex hardware implementation, using pulse compression and lower-rate sampling [7]. The performance of chirp signals for radar detection has been extensively studied in the literature and in text books [8], [9], and it will, therefore, not be addressed in this paper.

Chirps can also be used for communications, and this is the focus of this paper. Frequency-shift keying (FSK) modulated chirps have been proposed in [10], but, due to radar requirements, the data rate is limited by the chirp duration, which is usually much larger than the inverse of the bandwidth, resulting in a low spectral efficiency. The modulation with phase-shift keying (PSK) or quadrature-amplitude modulation

(QAM) has also been proposed in the literature [11], [12], but these papers consider a spread-spectrum system with low spectral efficiency. Chirps can be overlapped to increase the data rate, but suffer from inter-chirp interference (ICI), as the overlapping chirps are not orthogonal, except in very specific conditions [13]. Also in [13] the bit error rate (BER) performance of overlapping modulated chirps is derived, and linear equalization is proposed to compensate the ISI, showing that they can also be used close to the Nyquist signalling rates or even faster.

Individual chirps have constant amplitude, but the overlapping of chirps will increase the peak-to-average power ratio (PAPR) of the generated signal. This will increase the requirements on the linearity of radio-frequency (RF) circuits, with a consequent increase in implementation costs and loss of amplifier efficiency. With this in mind, in this paper we extend the analysis of [13] to consider the effect in the system performance of non-linearities in a power amplifier (PA) and in a low-noise amplifier (LNA).

The paper is organized as follows. In Section II we present our chirp-based waveform concept, and in Section III we present details of the PA and LNA models used to model the hardware imperfections in our study. These models are based in actual circuit design, also described in that section. Simulation results using these models are discussed in Section IV, and some concluding remarks are presented in Section V.

II. A CHIRP-BASED WAVEFORM FOR JOINT COMMUNICATIONS AND SENSING

The proposed waveform consists of transmission frames that can be used for radar, communications or both. At the beginning of each frame, M_p unmodulated non-overlapping chirps are transmitted. These can be employed for radar detection, but can also serve as a preamble for the communications part of the frame, facilitating synchronization and channel estimation. The number of preamble chirps is variable, depending on the requirements of a possible radar application. The preamble is followed by a sequence of M_d PSK/QAM-modulated chirps transmitting data. The number of modulated chirps depends of course on the requirements from the communication application, but we can also vary the interval between adjacent chirps. As shown in [13], shorter intervals increase the spectral efficiency, but also result in more inter-symbol interference among chirps, requiring more complex equalization techniques. The interval can thus be adapted to the BER and data-rate requirements of the particular application. This concept is depicted in Fig. 1.

As mentioned before, we focus on the communications part of the proposed waveform, which can be modelled as

$$s(t) = \sum_{i=0}^{M_d-1} d_i x(t - i\tau), \tag{1}$$

where d_i are complex-valued data symbols, with $E\left[|d_i|^2\right] = E_s$. $x(t)$ is an up-chirp pulse, which in baseband is given by

$$x(t) = \frac{1}{\tau_c} e^{j\pi B\left(-1+\frac{t}{\tau_c}t^2\right)}, \quad 0 \le t < \tau_c, \tag{2}$$

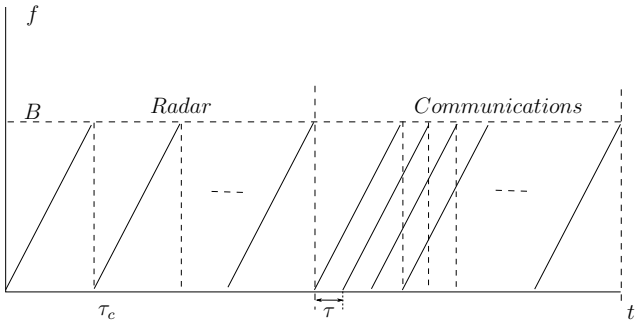

Fig. 1. The considered Joint Communications and Sensing Systems

with B and τ_c the sweep bandwidth and the chirp duration, respectively.

Considering an additive white Gaussian noise (AWGN) channel with a matched filter at the receiver, then the filter output is given by

$$y(t) = (s(t) + w(t)) * x^*(-t) \tag{3}$$

$$= \sum_{i=0}^{M_d-1} d_i r(t - i\tau) + n(t), \tag{4}$$

where $w(t)$ is the white Gaussian noise component with power spectral density $N_0/2$ and $n(t)$ is the corresponding filtered noise component.

$r(t)$ is the chirp autocorrelation function, which can be derived as [13]

$$r(t) = \frac{\sin\left(\pi Bt(1 - \frac{|t|}{\tau_c})\right)}{\pi Bt}, \quad |t| \le \tau_c. \tag{5}$$

If ideal synchronization is considered, the output of the matched filter at the time $t_k = k\tau$ is, therefore,

$$y_k = \sum_{i=0}^{M_d-1} d_i r\left((k-i)\tau\right) + n_k = d_k + v_k + n_k, \tag{6}$$

where $n_k = n(k\tau)$ and

$$v_k = \sum_{\substack{i=0 \\ i\neq k}}^{M_d-1} d_i r((k-i)\tau) \tag{7}$$

is the interchirp interference (ICI).

In [13] the authors have proposed a simple linear block equalizer to compensate for the ICI. This equalizer can be easily designed utilizing the closed-form interference matrix.

For a given frame, the sampled received signal can be represented as vector $\mathbf{y} = [y_0, y_1, \ldots, y_{M_d-1}]^T$, given by

$$\mathbf{y} = \mathbf{H}\mathbf{d} + \mathbf{n}, \tag{8}$$

where $\mathbf{d} = [d_0, d_1, \ldots, d_{M_d-1}]^T$, $\mathbf{n} = [n_0, n_1, \ldots, n_{M_d-1}]^T$ and the interference matrix $\mathbf{H}$ is defined as

$$\mathbf{H} = \begin{bmatrix} r_0 & r_{-1} & \cdots & r_{-(M_d-1)} \\ r_1 & r_0 & \cdots & r_{-(M_d-2)} \\ \vdots & \vdots & \ddots & \vdots \\ r_{M_d-1} & r_{M_d-2} & \cdots & r_0 \end{bmatrix}, \tag{9}$$

where $r_k = r(k\tau)$.

With this model, we can apply simple linear block equalization methods, for example, zero-forcing (ZF). Considering the eigenvalue decomposition $\mathbf{H} = \mathbf{U}\mathbf{\Sigma}\mathbf{U}^T$, then the transmitted data sequence can be estimated as

$$\hat{\mathbf{d}} = \mathbf{H}^{-1}\mathbf{s} = \mathbf{U}\mathbf{\Sigma}^{-1}\mathbf{U}^T\mathbf{s} \tag{10}$$

It was also shown in [13] that minimum mean-square error (MMSE) equalizer can also be employed, albeit with a negligible performance gain.

III. Modeling of Hardware Imperfections

In this section we describe the non-linearity models for both LNA and PA that are used in our simulations.

Most communication systems today utilize a carrier frequency below 10 GHz, even though automotive radars have been realized in 76-81 GHz. Due to overcrowded bands below 10 GHz, increasing complexity and limiting performance, there is a constant push to go to millimeter wave (mmWave) bands for communication devices. MmWave frequencies (by definition, above 30 GHz) may bring new frequency spectrum to use, but they will bring more challenges to be solved as well, namely, need of phased arrays to compensate for path losses, additional parasitic components in realization and additional development costs for advanced processes to fabricate the hardware. In order to reduce the development costs of hardware, and to overcome the limitations of devices at those frequencies, system co-design should be given highest priority. This will not only reduce the development cycles but it will provide a better optimized system. In our current work, the hardware performances are considered and integrated in the analysis, keeping the co-design principles in mind.

We have chosen a 2 GHz band around 60.48 GHz as one of the mmWave bands under consideration. Bands around 60 GHz have been long considered for communication systems, e.g., under IEEE 802.11ad [14] standard. More recently, besides 5G discussions, the 60 GHz band is also used for motion-sensing and gesture control applications in commercial products. Thus, this band is a strong candidate for research in joint communication and sensing domain.

Two front-end blocks are considered in our hardware models, a low noise amplifier and a power amplifier for low-power transceiver realization. The circuits are realized in 22 nm fully depleted silicon-on-insulator (FDSOI) process from Global Foundries. The device layouts are extracted and post-layout simulations are considered here. Their design principles and simulated behaviour are presented below.

A. Low-noise amplifier

Fig. 2 shows the schematic of a two-stage single-ended LNA. The amplifier utilizes inductive degeneration in both stages to increase stability and ease of matching for devices. The input matching is realized by an inductive transmission line. Inductive degeneration improves the linearity by forming a negative series feedback. The input stage uses common-source for better noise performance, and the second stage is the gain stage using cascade device configuration. Both input and output ports are matched to 50 Ω. The inter-stage tuning and the output matching are both realized using transmission lines. The transmission lines used in the design are high-Q coplanar waveguide transmission lines with shielding. The sizing of the transistors is done to reduce the noise contribution of each transistor by biasing it close to the current-gain cutoff frequency f_T [15]. The LNA is tuned to the specific bandwidth to avoid out-of-band signals influencing the receiver chain, as it is almost impossible to integrate input filters after antenna at these frequencies.

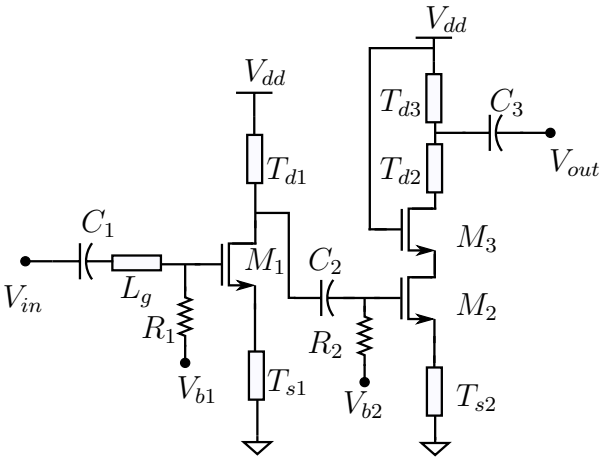

Fig. 2. 61GHz LNA Schematic

B. Power amplifier

The schematic of the power amplifier is shown in Fig. 3. The 2-stage power amplifier is realized using common source configuration with source degeneration in both stages. Coplanar waveguide transmission lines with ground shielding are used for all matching. The transistors are matched to deliver higher power outputs over a very wide bandwidth and the transistor gain roll-off is not fully compensated to avoid narrow-band performance.

C. LNA and PA simulation results

Fig. 4 depicts the frequency response plots of both LNA and PA. The LNA reports a gain of 22 dB and the PA achieves a gain of 8.8 dB at 61 GHz. The low-noise amplifier draws a total 20 mA current from a 0.8 V supply providing 4.6 dB noise figure and 19 dB gain over a 3 GHz bandwidth. The 1 dB bandwidth of the wideband PA is larger than 5 GHz.

Fig. 5 shows the AM/AM conversion model of both LNA and PA, including their 1 dB compression point ($P_{1\text{dB}}$). The LNA achieves $P_{1\text{dB}} = -18.34$ dBm output. The power amplifier draws 22 mA current from 0.8 V yielding $P_{1\text{ dB}} = -4$ dBm and 8 dBm saturated output power.

IV. Simulation Results

We have simulated the waveform and equalizer presented in II, considering the PA and LNA models described in Section

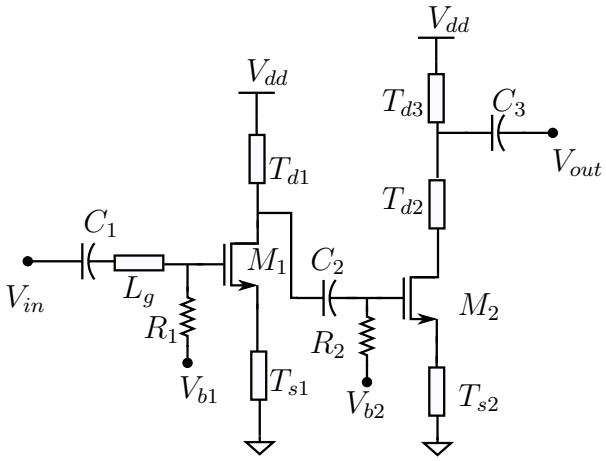

Fig. 3. 61GHz PA Schematic

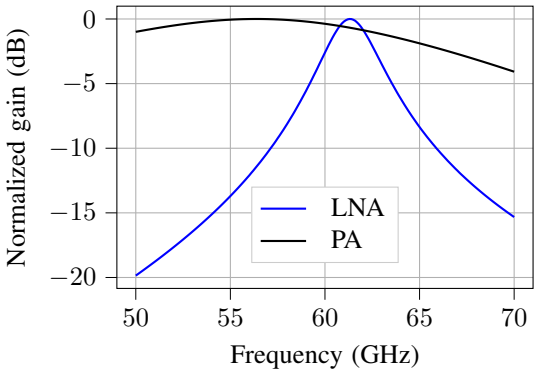

Fig. 4. Frequency response of PA and LNA

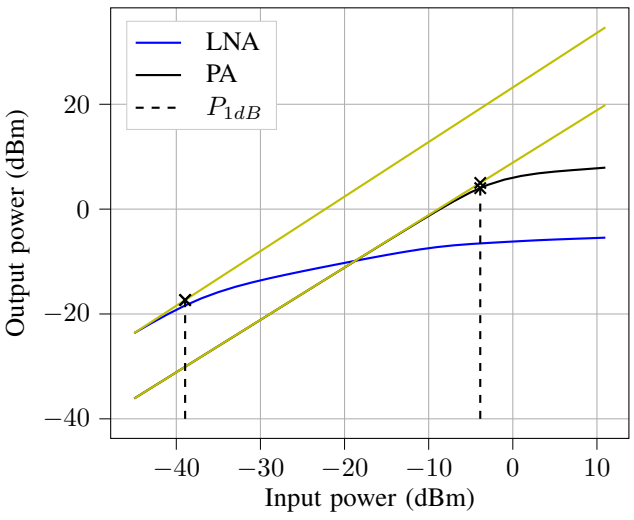

Fig. 5. AM/AM conversion model of PA and LNA (1 dB compression point marked)

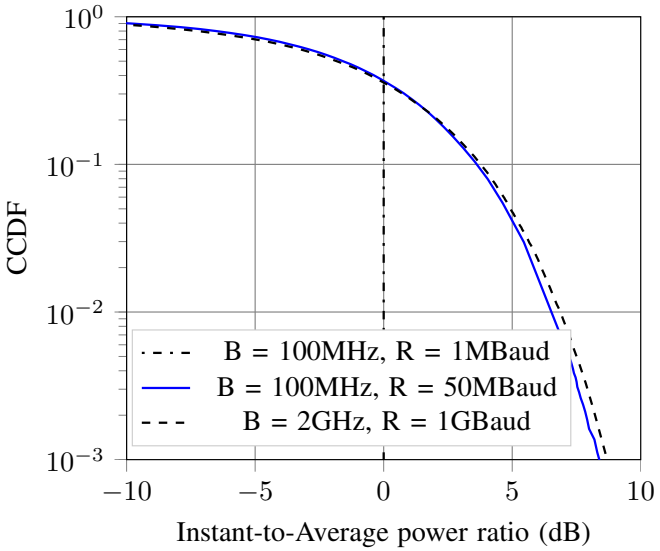

Fig. 6. Empirical distribution of the instant transmit power

III. As mentioned before, we focus on the communications performance of the proposed JC&S waveform, and consider perfect synchronization and a single-path channel without fading. No channel coding is considered in all simulations, and we transmit frames consisting of $M_d = 1000$ data symbols each.

In this whole section we consider chirps with length 1 μs, with bandwidth either $B = 100$ MHz or $B = 2$ GHz. Results were obtained with our link-level simulator HermesPy [16].

First, though, we investigate the power variation of the transmitted signal with different parameters, since this is the main factor affecting the performance with non-linear devices. In Fig. 6 we display the empirical complementary cumulative distribution function (CCDF) of the instant power ratio, as a ratio to the average power, with BPSK modulation. As expected, we notice that non-overlapping chirps (symbol rate $R = 1$ Mbaud) have a constant amplitude, and that the signal presents a larger variation of the instant power as the number of overlapping chirps $N_{ol} = \lceil \tau_c/\tau \rceil$ increases.

In Fig. 7 we simulate a system with bandwidth $B = 100$ MHz and 16-QAM modulation, with different symbol rates R_s, and display its bit error rate (BER). For a symbol rate $R_s > 1/\tau_c$ the chirps will overlap, with a consequent interchirp interference (ICI). We show the performance without equalization to show the effect of ICI. However, a simple ZF block equalizer can effectively compensate ICI, attaining the same performance as the theoretical performance in an AWGN channel for $R_s = B/10 = 10$ MHz, or just with a small performance loss, even at the Nyquist signalling rate, $R_s = B = 100$ MHz. Unless otherwise stated, all other BER curves in this paper consider ZF equalization. .

Further, we simulated the effect of a non-linear PA, following the model from Section III-B. We have simulated with different input backoff (IBO) values, defined as the

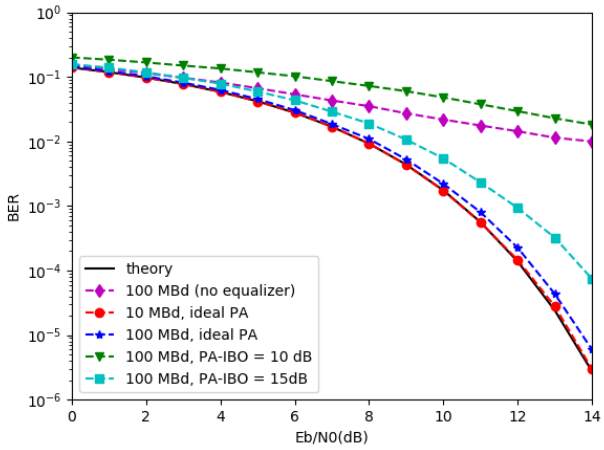

Fig. 7. System performance with $\tau_c = 1\,\mu$s, $B = 100$ MHz, 16-QAM (ideal LNA)

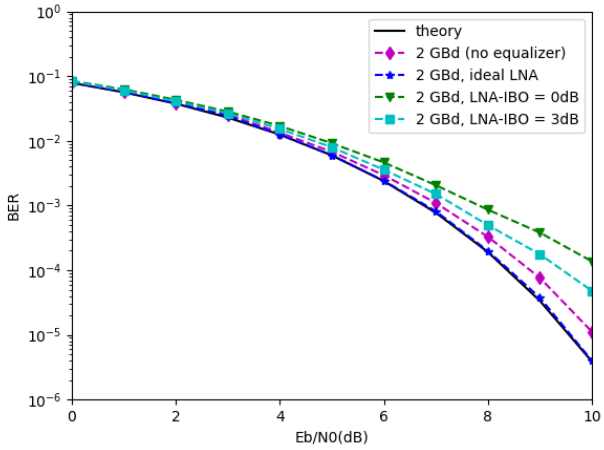

Fig. 8. System performance with $\tau_c = 1\,\mu$s, $B = 2$ GHz, $R_s = 2$ GBd QPSK (ideal PA)

difference between the 1-dB compression point $P_{1\text{dB}}$ and the average signal power. Non-linearities only become important with power variations, which, as shown in Fig. 6, occur with overlapping chirps, i.e., with data rates $R_b > 1/\tau_c$. We see that as the backoff decreases, the signal suffers higher distortion and the performance deteriorates.

We also simulated a system with bandwidth $B = 2$ GHz and QPSK, and the results are displayed in Fig.8. As shown in [13], the ICI at the Nyquist signalling rate decreases with an increasing time-bandwidth product $B\tau_c$, and the ZF equalizer can effectively compensate the the ICI at the Nyquist rate.

We also investigated the effect of non-linear components in the system performance with this high bandwidth. Now, however, we assume that the power amplifier is linear, and investigate the impact of the considered LNA. As we can observe from the Fig. 8, the system can operate with a lower LNA backoff, when compared with the PA impairments.

V. Conclusions

In this paper we have presented a chirp-based waveform, that, in addition to radar detection, can also be used for data transmission. Such a waveform can be a key enabler for offering radar as a service in future wireless communications systems, and understanding its performance including realistic hardware realizations is essential. With that in mind, we have presented the circuit design of a suitable power amplifier and a low-noise amplifier , with the corresponding non-linear behaviour. The performance of the chirp waveform was simulated using these circuits, allowing us to derive some design guidelines for future chirp-based joint communications and sensing systems.

References

[1] C. de Lima *et al.*, "6G white paper on localization and sensing [white paper]," . University of Oulu, Tech. Rep. 6G Research Visions, No. 12, Jun. 2020. [Online]. Available: http://urn.fi/urn:isbn:9789526226743

[2] F. Liu *et al.*, "Joint radar and communication design: Applications, state-of-the-art, and the road ahead," *IEEE Transactions on Communications*, vol. 68, no. 6, pp. 3834–3862, 2020.

[3] W. Buller *et al.*, "Radar congestion study," National Highway Traffic Safety Administration, Tech. Rep. DOT HS 812 632, Sep. 2018.

[4] B. Dekker *et al.*, "Gesture recognition with a low power fmcw radar and a deep convolutional neural network," in *2017 European Radar Conference (EURAD)*, 2017, pp. 163–166.

[5] L. Zheng, M. Lops, Y. C. Eldar, and X. Wang, "Radar and communication coexistence: An overview: A review of recent methods," *IEEE Signal Processing Magazine*, vol. 36, no. 5, pp. 85–99, 2019.

[6] C. Sturm and W. Wiesbeck, "Waveform design and signal processing aspects for fusion of wireless communications and radar sensing," *Proceedings of the IEEE*, vol. 99, no. 7, pp. 1236–1259, 2011.

[7] I. Bilik, O. Longman, S. Villeval, and J. Tabrikian, "The Rise of Radar for Autonomous Vehicles: Signal processing solutions and future research directions," *IEEE Signal Processing Magazine*, vol. 36, no. 5, pp. 20–31, 2019.

[8] M. Richards, *Principles of Modern Radar: Basic Principles (1st Edition)*. Scitech Publishing, 2010.

[9] B. R. Mahafza, *Radar Systems Analysis and Design Using Matlab (3rd Edition)*. CRC Press, 2013.

[10] S. Dwivedi, A. N. Barreto, P. Sen, and G. Fettweis, "Target detection in joint frequency modulated continuous wave (fmcw) radar-communication system," in *16th International Symposium on Wireless Communication Systems (ISWCS)*, 2019, pp. 277–282.

[11] A. Springer *et al.*, "A wireless spread-spectrum communication system using SAW chirped delay lines," *IEEE Trans. Microwave Theory Techn.*, vol. 49, no. 4, pp. 754–760, Apr. 2001.

[12] T. Yoon, S. Ahn, S. kim, and S. Yoon, "Performance analysis of an overlap-based CSS system," in *IEEE Intl. Conf. Adv. Commun. Technology (ICACT)*, Gangwon-Do, South Korea, 2008.

[13] T. M. Pham, A. N. Barreto, and G. P. Fettweis, "Efficient communications for overlapped chirp-based systems," *IEEE Wireless Communications Letters*, pp. 1–1, 2020.

[14] M. Boers *et al.*, "A 16TX/16RX 60 GHz 802.11ad chipset with single coaxial interface and polarization diversity," *IEEE Journal of Solid-State Circuits*, vol. 49, no. 12, pp. 3031–3045, 2014.

[15] B. Afshar and A. M. Niknejad, "X/Ku band CMOS LNA design techniques," in *IEEE Custom Integrated Circuits Conference 2006*, 2006, pp. 389–392.

[16] "HEterogeneous Radio MobilE Simulator in Python (HermesPy) - https://github.com/barkhausen-institut/hermespy."